Jefferson Lab PAC13
Proposal Cover Sheet

This document must be received by close of business Thursday, **December 18, 1997** at:

Jefferson Lab
User Liaison Office,
Mail Stop 12B
12000 Jefferson Avenue
Newport News, VA
23606

Experimental Hall: A
Days Requested for Approval: 10

☒ **New Proposal Title:**
☐ **Update Experiment Number:**
☐ **Letter-of-Intent Title:**
(Choose one)

Proposal Physics Goals
Indicate any experiments that have physics goals similar to those in your proposal. Structure of Proton

Approved, Conditionally Approved, and/or Deferred Experiment(s) or proposals:
E93050

Contact Person
Name: BOGDAN WOJTSEKHOWSKI
Institution: TJNAF
Address: 1200 Jefferson Ave
Address:
City, State, ZIP/Country: N-News, VA 23606
Phone: 757-2697191 **Fax:** 269-7363
E-Mail: BogdanW@CeBaf.gov

JLab Use Only
Receipt Date: 11/18/97 PR 97-108
By: JX

LAB RESOURCES LIST

JLab Proposal No.: _____ Date _____

(For JLab ULO use only.)

List below significant resources — both equipment and human — that you are requesting from Jefferson Lab in support of mounting and executing the proposed experiment. Do not include items that will be routinely supplied to all running experiments such as the base equipment for the hall and technical support for routine operation, installation, and maintenance.

Major Installations *(either your equip. or new equip. requested from JLab)*

Lead Glass Calorimeter (~650 blocks)

Sweep Magnet

New Support Structures:

Movable platforms for Calorimeter and Magnet

Data Acquisition/Reduction

Computing Resources:

New Software:

Major Equipment

Magnets: $\int Bdl \approx 0.1$ Tm 30cm gap Sweep Magnet

Power Supplies: for magnet

Targets:

Detectors: ~650 blocks Lead Glass Calorimeter and MWPC

Electronics: ~700 ADC channels and ~50 TDC channels

Computer Hardware:

Other:

Other:

BEAM REQUIREMENTS LIST

JLab Proposal No.: _____ Date: _____

Hall: A Anticipated Run Date: 10 days PAC Approved Days: _____

Spokesperson: WOJTSEKHOWSKI Hall Liaison: _____
Phone: 757 269 7191
E-mail: BOGDANW@CEBAF.GOV

List all combinations of anticipated targets and beam conditions required to execute the experiment. (This list will form the primary basis for the Radiation Safety Assesment Document (RSAD) calculations that must be performed for each experiment.)

Condition No.	Beam Energy (MeV)	Mean Beam Current (μA)	Polarization and Other Special Requirements (e.g., time structure)	Target Material (use multiple rows for complex targets — e.g., w/windows)	Material Thickness (mg/cm²)	Est. Beam-On Time for Cond. No. (hours)
1	3	10	—	LH & Cu	1500	1.8
2	4	10	—	LH & Cu	1500	5.4
3	5	10	—	LH & Cu	1500	86
4	6	10	—	LH & Cu	1500	69

The beam energies, E_{Beam}, available are: $E_{Beam} = N \times E_{Linac}$ where N = 1, 2, 3, 4, or 5. E_{Linac} = 800 MeV, i.e., available E_{Beam} are 800, 1600, 2400, 3200, and 4000 MeV. Other energies should be arranged with the Hall Leader before listing.

HAZARD IDENTIFICATION CHECKLIST

JLab Proposal No.: _____ Date: _____
(For CEBAF User Liaison Office use only.)

Check all items for which there is an anticipated need.

Cryogenics
- ____ beamline magnets
- ✓ analysis magnets
- ✓ target
  - type: _____
  - flow rate: _____
  - capacity: _____

Electrical Equipment
- ✓ cryo/electrical devices
- ____ capacitor banks
- ✓ high voltage
- ____ exposed equipment

Radioactive/Hazardous Materials
List any radioactive or hazadorous/ toxic materials planned for use:
_____
_____
_____
_____

Pressure Vessels
- ____ inside diameter
- ____ operating pressure
- ____ window material
- ____ window thickness

Flammable Gas or Liquids
- type: LH_2 (target)
- flow rate: _____
- capacity: _____

Drift Chambers
- type: VDC (HRS)
- flow rate: _____
- capacity: _____

Other Target Materials
- ___ Beryllium (Be)
- ___ Lithium (Li)
- ___ Mercury (Hg)
- ✓ Lead (Pb)
- ___ Tungsten (W)
- ___ Uranium (U)
- ___ Other (list below)

_____
_____

Vacuum Vessels
- ____ inside diameter
- ____ operating pressure
- ____ window material
- ____ window thickness

Radioactive Sources
- ____ permanent installation
- ____ temporary use
- type: _____
- strength: _____

Large Mech. Structure/System
- ____ lifting devices
- ____ motion controllers
- ____ scaffolding or
- ✓ elevated platforms

Lasers
- type: _____
- wattage: _____
- class: _____

Installation:
- ____ permanent
- ____ temporary

Use:
- ____ calibration
- ____ alignment

Hazardous Materials
- ____ cyanide plating materials
- ____ scintillation oil (from)
- ____ PCBs
- ____ methane
- ____ TMAE
- ____ TEA
- ____ photographic developers
- ____ other (list below)

_____
_____

General:

Experiment Class:
- ✓ Base Equipment
- ____ Temp. Mod. to Base Equip.
- ____ Permanent Mod. to Base Equipment
- ____ Major New Apparatus

Other: Lead Glass Calorimeter

Exclusive Compton Scattering on The Proton

J. P. Chen, E. Chudakov, C. DeJager, P. Degtyarenko,
R. Ent, J. Gomez, O. Hansen, C. Keppel, M. Kuss, J. LeRose,
M. Liang, R. Michael, J. Mitchell, S. Nanda, P. Rutt,
A. Saha, B.Wojtsekhowski (co-spokesman and contact person)
TJNAF, Newport News VA

B. S. Bains, M. Bouwhuis, R. J. Holt, N.C.R. Makins,
A. M. Nathan (co-spokesman), S.E. Williamson
University of Illinois at Urbana-Champaign, Urbana IL

G. Dodge, C. Hyde-Wright (co-spokesman),
A. Radyushkin, L. B. Weinstein, P. Ulmer
Old Dominion University, Norfolk VA

P. Bosted
The American University, Washington DC

J. M. Finn
College of William and Mary, Williamsburg VA

R. Gilman
Rutgers University, New Brunswick NJ

J. Berthot, P. Bertin, V. Breton, H. Fonvieille, Y. Roblin
University Blaise Pascal/IN2P3, Aubie're FRANCE

W. Bertozzi, K. Fissum, J. Gao, S. Gilad, N. Liyanage,
D. Rowntree, J. Zhao, Z. Zhou
Massachusets Institute of Technology

G. Chang
University of Maryland

A. Ketikyan, A. Shahinyan, H. Voskanyan
Yerevan Physics Institute

W. Boeglin, P. Markowitz
Florida International University

J.Hines, G.Strobel, J.Templon
University of Georgia

G. Feldman
George Washington University

C. L. Morris
Los Alamos National Laboratory

V. Gladyshev, R. A. Lindgren
University of Virginia

J. Calarco, W. Hersman
University of New Hampshire

A. Gasparian
Hampton University
(December 21, 1997)

Abstract

We propose measurements at 3 – 6 GeV of Compton scattering $\gamma + p \rightarrow \gamma + p$ at large perpendicular momentum transfer to the proton. Recent theoretical developments offer the possibility of a unified treatment of high energy Compton scattering, elastic form factors, and deep inelastic scattering. We will use an untagged bremsstrahlung beam in Hall A with coincidence detection of the recoil proton and scattered photon. The proton will be detected in one of the HRS spectrometers, and the photon will be detected in a large-area, multi-segment Pb-Glass calorimeter.

I. INTRODUCTION

Compton scattering ($\gamma+p \to \gamma+p$) at high energy (s) and high momentum transfer (t) is a potentially powerful probe of the short-distance structure of the nucleon. It is a natural complement to other studies of nucleon structure, including high Q^2 measurements of the elastic electric and magnetic form factors, virtual Compton scattering, and deep inelastic scattering. In this proposal we present a program of Compton scattering from the proton up to an energy 6 GeV. We begin with a discussion of the physics motivation (Sec. II) in which we will argue that the range of s and t accessible to TJNAF is one that potentially provides a bridge between perturbative and non-perturbative QCD treatments of the short-distance structure of the proton. We next discuss the experimental aspects in Sec. III, including the necessary equipment, expected counting rates, and backgrounds. Additional sections include the beam request/run plan (Sec. IV) and collaboration issues Sec. V). We conclude with a brief discussion of possible future developments (Sec. VI).

We propose measurements of Compton scattering using an untagged bremsstrahlung beam in Hall A, with detection of the recoil proton in one of the HRS spectrometers in coincidence with the scattered photon in a Pb-Glass Calorimeter which we will construct for this experiment. Our kinematics for the incident and scattered photon and proton are defined, respectively, as follows:

$$\gamma + p \longrightarrow \gamma + p \tag{1}$$

$$q_\mu + P_\mu \longrightarrow q'_\mu + P'_\mu \tag{2}$$

It is also convenient to describe the reaction in terms of the Mandelstam invariants:

$$s = (q+p)^2_\mu = \left[M^2 + 2qM\right]_{\rm Lab} \tag{3}$$

$$t = (q-q')^2_\mu = 2qq'(1-\cos\theta_{\gamma\gamma}) = \frac{s}{2}\left[1-\frac{M^2}{s}\right]^2 [1-\cos\theta_{cm}] \tag{4}$$

$$u = (q-P')^2_\mu = (P-q')^2_\mu = M^2 - t - (s-M^2) \tag{5}$$

We will also refer to the perpendicular momentum transfer

$$p_\perp = p' \sin\theta_{\gamma p} = q' \sin\theta_{\gamma\gamma}, \tag{6}$$

where $\theta_{\gamma p}$ and $\theta_{\gamma\gamma}$ are the angles between the recoil proton and the incident beam, and the scattered photon and the incident beam, respectively. Notice that Eq. 6 is equally valid in the laboratory or Center-of-Mass (CM) frames of reference. The focus of this proposal is on Compton scattering at large $p_\perp$.

For extreme small angle production, there exists an extensive experimental literature on high energy Compton scattering and coherent π^0 production on the proton. [1] However, the data of Shupe *et al.*, [2] from Cornell are the only data at large scattering angles. These are illustrated in Fig. 1 & 2. The data include photon energies from 2.0 GeV to 6.0 GeV, but there are only a total of 3 points at 5 and 6 GeV, each with 20% to 40% statistics.

Our proposed kinematics are listed in Table I. At endpoint energies of 5 and 6 GeV, we will measure a broad angular distribution. At 3 and 4 GeV, we will measure at $\theta_{cm} =$ 90°, 110° to complement and improve upon the existing data of Shupe *et al.* [2] At all points,

we will make measurements with at least 5% statistical precision (including all background subtractions) and 6% systematic errors. The physics motivation for this study is discussed in detail in the following section. By way of illustration, we note that from general principles of field theory, the differential cross section $d\sigma/dt$ at large $p_\perp$ is expected to scale as s^{-6} at fixed θ_{cm}. [3] These proposed measurements will allow us to study this scaling law (or the approach to scaling) over a factor of 300 variation in the cross section.

II. PHYSICS MOTIVATION

A. Hard Scattering limit of Compton Scattering

We seek a unified description of elastic electroweak scattering $N(e,e')N$, elastic Compton scattering $p+\gamma \to p+\gamma$ and elastic virtual Compton scattering $ep \to ep\gamma$ at high energy. Elastic electron scattering measures a ground state current density. Elastic Compton scattering (real or virtual) measures a density-density correlation. In Compton scattering, the quark current couples twice to the system; the intermediate state contains *a priori* the full complexity of a strongly interacting system. Thus in general, elastic Compton scattering depends not only on the ground state structure, but also on an integral over the structure of all excited states. Real Compton scattering, $\gamma p \to \gamma p$, virtual Compton scattering (VCS) $ep \to ep\gamma$ and deep inelastic electron scattering (DIS) $ep \to eX$ are all described theoretically by the generalized Compton amplitude $\gamma p \to \gamma p$ (with real or virtual photons in either or both the initial and final states). There are now clear theoretical suggestions that the introduction of at least one hard scale allows one to factorize the Compton amplitude into the ground state matrix element of a short distance (and therefore perturbative) reaction kernel. This is illustrated in Fig. 4(b)&(c) in the large Q^2 case for DIS and VCS, and in Fig. 5 for $p_\perp^2$ large in Compton scattering. In this proposal, we seek to study this hypothesis of factorization in the hard scattering domain of large $p_\perp^2$. This is obtained experimentally at high energy (equivalently large s) and wide angles: to exclude the diffractive regions of small $-t$ and small M^2-u requires both θ_{cm} and $\pi-\theta_{cm}$ large.

In the hard scattering limit of any two-body process, the quark counting rule of Brodsky & Farrar [3] predicts scaling laws of the form,

$$d\sigma/dt = f(\theta_{cm})s^{2-n}, \tag{7}$$

where n is the number of elementary constituents in the reaction. In the Compton case, $n=8$ (three quarks and a photon in the initial and in the final state). The experimental results from the Shupe data are:

$$\begin{aligned} p(\gamma,\gamma p)|_{\theta_{cm}=60^\circ} \qquad & \frac{d\sigma}{dt} \propto s^{-6.0\pm0.3} \\ p(\gamma,\gamma p)|_{\theta_{cm}=90^\circ} \qquad & \frac{d\sigma}{dt} \propto s^{-7.1\pm0.4} \\ p(\gamma,\gamma p)|_{\theta_{cm}=105^\circ} \qquad & \frac{d\sigma}{dt} \propto s^{-6.2\pm1.4} \end{aligned} \tag{8}$$

The statistical error bars of 16%-40% are reflected in the error bars on the exponents in Eq. 8. In the present proposal, with 8% overall errors bars and a 6 GeV endpoint energy,

the error bar on the exponent of the Compton scaling law can be reduced to ± 0.1, and the range of s^6 at $\theta_{cm} = 90°$ extended by nearly a factor of three.

For large scattering angles, due to the superposition of many angular momenta in the intermediate state, each channel of Fig. 3 can be expected to contribute a random phase to the Compton amplitude. Consequently the contribution of any individual hadronic diagrams is suppressed in the hard scattering limit. In addition, the large transverse momentum transfer limits the propagating intermediate state to short distances: Compton scattering in this case is therefore dominated by the partonic diagrams of Fig. 5. In these diagrams, the intermediate state is perturbative; it does not have soft interactions.

In Fig. 5(a) & (b), the two photons couple to a single quark (or anti-quark). The spectator in general can include the full valence and sea degrees of freedom of the proton. In Fig. 5(c) the two photons couple to two different partons, This diagram will be suppressed, however, because q and q' both have large transverse momentum (relative to $q - q'$).

The high energy, wide angle Compton scattering process leads to a hierarchy of approximations:

1) Perturbative intermediate state: No soft interactions in intermediate state.

2) Neglect of higher Fock-space configurations in initial state (elementary $|qqq>$ state only).

3) Neglect of quark perpendicular momentum components (relative to momentum transfer direction $\vec{q} - \vec{q}'$) in initial and final states.

4) Dominance of diagrams with perturbative two-gluon exchange.

The validity of each approximation does not depend on the others lower in the list. There are three approaches to the hard scattering domain:

- Perturbative QCD (pQCD)
- Di-quark Model
- Feynman Mechanism

These three differ in how the momentum transfer t is shared by the proton constituents. In fact, they are listed above in order such that the momentum transfer is shared by three (pQCD), two (di-quark), or one (Feynman) of the constituents of the proton, respectively. PQCD and the Feynman mechanism each offer a general framework for understanding Compton scattering. Within each framework, models of the proton structure must be applied.

B. Perturbative QCD

In the perturbative QCD (pQCD) calculations of Compton scattering [5,4], the Compton process samples only the elementary 3-quark Fock space configuration of the proton. The perpendicular momentum components of the three elementary quarks are integrated out of the wave function, leaving the distribution amplitude (DA) $\phi(x_1, x_2, x_3)$ of the light-cone

momentum fractions of the three quarks. The light cone z-direction is along $\vec{q}-\vec{q}'$. Neglecting the perpendicular momenta of the quarks is equivalent to writing the wave function as a δ-function in the transverse coordinates. The VCS amplitude is written (schematically) as:

$$T^{\mu\nu}(s_q, Q^2, t) = \int d^3x d^3y \phi(x) \hat{K}^{\mu\nu}(x,y) \phi(y). \tag{9}$$

$\hat{K}^{\mu\nu}(x,y)$ is the hard scattering kernel that includes all distinct diagrams in which two photons couple to three quarks which exchange two perturbative gluons. The exchange of perturbative gluons shares the momentum transfer between the three quarks. The gluon propagators ensure that the scaling law Eq. 7 is produced, up to logarithmic evolution. Numerically, the integral in Eq. 9 is dominated by the endpoints, corresponding to the exchanged gluons close to their mass shell. This calls into question the internal consistency of the pQCD approach, at least at finite s and t. These difficulties may be partially alleviated if the transverse momentum dependence (or equivalently the transverse size) is included explicitly [6]. However, restoring the transverse separation of the quarks strongly suppresses perturbative gluon exchange, and reduces the predicted cross sections well below the existing data for both Compton scattering and the elastic form factors (Fig. 1 and Ref. [7], [8])

C. Di-Quark Model

In the di-quark model of Kroll *et al.*, the high momentum transfer $p(e,e')p$ or $p(\gamma,\gamma p)$ reactions sample a Fock-space consisting of a quasi-elementary quark and di-quark (both scalar and vector) [9,10]. The relative perpendicular momentum between the quark and di-quark components is neglected (similar to the pQCD calculations). In this model, the momentum transfer to the proton is shared by perturbative gluon exchange between the quark and di-quark and by the internal di-quark structure, described by a di-quark form factor. The di-quark form factor is constructed so that asymptotically the di-quark model agrees with the pQCD calculation.

The di-quark calculations of Kroll *et al.* [9,10] provide an interesting interpretation of the existing real Compton scattering data [2]. In particular, the scaling violations suggested by the present data are reproduced by the model. In the di-quark model, since the proton has only two constituents, Eq. 7 should be modified to

$$d\sigma/dt = s_q^{-4} |F(-t)|^2 f_{\mathrm{di-quark}}(\theta_{cm}), \tag{10}$$

where $F(-t)$ is the di-quark form factor. In the forward direction (small t), the Compton process does not resolve the substructure of the di-quark ($F(-t) \approx 1$). Hence the predicted cross section should scale as s^{-4}. In fact both the data and the model fall less rapidly than s^{-6} in the forward direction. On the other hand at large t ($\theta_{cm} \geq 90°$) the di-quark form factors are important. The scalar and vector di-quark form factors are monopole and dipole, respectively:

$$F_S(-t) = Q_S^2 \left/ [Q_S^2 - t] \right., \qquad F_V(-t) = \left[Q_V^2 \left/ [Q_V^2 - t] \right. \right]^2. \tag{11}$$

Since $-t \approx (s_q/2)(1-\cos\theta_{cm})$, at large t the scalar di-quark terms in the cross section will fall like s_q^{-6} at fixed θ_{cm} and the vector di-quark terms in the cross section will fall like s_q^{-8}.

At $\theta_{cm} = 90°$ both the data and the model cross sections fall faster than s_q^{-6} (Eq. 8). In this case the vector di-quark is modeling the non-valence (and helicity violating) structure in the proton. The parameters of the di-quark model are constrained primarily by the elastic form factors $G_{E,M}^{p,n}$ at $Q^2 > 1$ GeV^2. The improved data set we seek to obtain will help determine whether it is possible to obtain a consistent phenomenological interpretation of both elastic electron and photon scattering.

D. Feynman Mechanism

Before the advent of QCD, Feynman conjectured that high momentum transfer exclusive processes are dominated by ground state configurations in which a single parton carries a (light-cone) momentum fraction near unity [11]. In the context of QCD, it has been conjectured that the Feynman mechanism, rather than perturbative gluon exchange will dominate hard scattering processes at presently accesssible energies that are well below asymptopia. [12,7] It is the soft part of the wave-function ($x_{i_0} \to 1$) rather than perturbative gluon exchanges that provide the main mechanism for absorbing the momentum transfer. This approach has been applied to the proton form factor [8], in this case, the transverse momentum of the constituents is modeled by a wave function of the form:

$$\psi(p_1, p_2, p_3) = \phi(x_1, x_2, x_3) e^{-\sum_i \frac{k_{i,\perp}^2}{x_i \Lambda^2}} \tag{12}$$

$$\approx x_1 x_2 x_3 \delta(1 - (x_1 + x_2 + x_3)) e^{-\sum_i \frac{k_{i,\perp}^2}{x_i \Lambda^2}} \tag{13}$$

If one of the constituents carries nearly all of the longitudinal momentum, then the others have nearly zero momentum fractions. The wave function has the approximate form $\prod_i^n x_i$. Thus the Feynman mechanism is dominated by the Fock space configuration with the fewest number of constituents (fewest number of factors $x_i \approx 0$) in the wave function.

The quark kernel in Fig. 5(a) has the form of the Klein-Nishina formula for γ-fermion Compton scattering. The two photons couple to the quark in Fig. 5(a) & (b) at two separate space-time points. However, in the hard scattering limit, the large transverse momentum of q and q' (relative to $q - q'$) will force the two vertices to a common point. In this case, the hard scattering Compton amplitude is proportional to the Klein-Nishina amplitude for each quark flavor times the usual flavor dependent vector and axial vector form factors of the proton. The generates a different scaling prediction: at fixed t, the s dependence should be given by the Klein-Nishina (KN) formula [15]

$$\frac{d\sigma(\gamma,\gamma)}{dt} \propto \left(\frac{d\sigma}{dt}\right)_{\rm KN} \left[\sum_f e_f^2 F_f(-t)\right]^2 . \tag{14}$$

This provides a way of modeling the hard scattering Compton amplitude independent of any assumption about the Fock space configurations of the proton wave function. The soft physics is contained entirely in the flavor-dependent form factors. These are similar to the form factors measured in elastic electron scattering except that the Compton scattering amplitude is sensitive to quark matrix elements weighted by the quark charge squared whereas the elastic electron form factors are weighted by the quark charge. Thus Compton scattering

is directly sensitive to the flavor structure of the proton elastic form factor in a different way from electro-weak scattering, thereby providing another tool (along with parity-violating electron scattering) for decomposing the flavor structure.

In summary, we wish to test the hypothesis of factorization of the Compton amplitude (and exclusive processes in general) at large $p_\perp$. This hypothesis leads to a series of approximations, enumerated above, each with different predictions for the behavior of the cross section as a function of s and t or $\theta_{\gamma\gamma}$. In the context of pQCD, our data can be used to obtain improved constraints on the DA $\phi(x_1, x_2, x_3)$. [17,16] The Feynman mechanism gives us a different scaling law to test (Eq. 14) and provides a direct link with elastic form factors. In general, the models described above are tested as a function of s, and interpreted to constrain the proton structure as a function of $\theta_{\rm CM}$ or t. Thus we need new and improved data over a wide range in both s and $\theta_{\rm CM}$

III. EXPERIMENTAL ASPECTS

A. Overview

We propose to measure differential cross sections for Compton scattering from the proton $p(\gamma, \gamma' p)$ at incident photon energies between 3 and 6 GeV and at a variety of CM scattering angles. A plan view of the experimental setup in Hall A is shown in Fig. 6. The high duty factor electron beam impinges on a 6% copper radiator located just upstream of the scattering target. The mixed beam of electrons and bremsstrahlung photons is incident on a 15-cm target of liquid Hydrogen. The recoil proton is detected in one of the HRS magnetic spectrometers. The associated scattered photon is detected in an electromagnetic calorimeter consisting of 625 Pb-Glass blocks in a 1 m x 1 m array. Only the upper portion of the continuous bremsstrahlung beam is used. A combination of veto detector and sweep magnet serve to reduce the background from charged particles, principally electrons, in the calorimeter. The second HRS spectrometer will operate at a fixed angle and serve as a luminosity monitor.

The kinematics we have chosen to investigate is shown in Fig. 7 as well as in Tables I and II. Specifically, we propose 17 measurements that are arranged in order to study the s-dependence of the cross section at two fixed $\theta_{cm} = 90°$ and 110° and at fixed $-t \sim 3.2$ GeV^2, as well as the t-dependence of the cross section at the fixed s corresponding to 5 and 6 GeV beams. One fixed angle $\theta_{cm} = 90°$ was chosen because it corresponds to the largest transverse momentum. The angular limits of the 6 GeV measurements are dictated on the low end ($\theta_{cm} = 70°$) by the need to keep the photon detector at a laboratory angle no smaller than 20° due to the severe increase in bremsstrahlung background below that angle, and on the high side by the maximum momentum one can detect with the HRS (4.5 GeV). The broadest angular coverage will be done at 5 GeV, where we will cover the region θ_{cm}=60°-135°. Of the proposed measurments, the 3 and 4 GeV points overlap with the best of the Cornell work. The bulk of the points go beyond the Cornell measurements, which have only 3 points at energies $\geq$ 5 GeV and overall accuracy of 30%.

An essential feature of the experiment is to use the kinematic correlation between the scattered photon and the recoil proton in the $p(\gamma, \gamma' p)$ reaction to remove one of the principal sources of background, namely, photons from the decay of neutral pions produced in the

$p(\gamma, \pi^0 p)$ reaction. This requires the best possible angular resolution from both the recoil spectrometer and the photon detector. The technique we will use is conceptually identical to that used in the Cornell experiment. However, the combined effects of a high quality, high duty factor electron beam, a state-of-the-art magnetic spectrometer, and better segmentation in the photon detector should allow significantly better measurements in the range of s and t already covered by Cornell, as well as extensions beyond that. The equipment would also be suitable for measurements at higher energies, should those energies become available at TJNAF in the future.

B. Electron/Photon Beam

The TJNAF CW electron beam will be incident on a 6% copper radiator located approximately 0.7 m upstream of the target. Multiple scattering in the radiator will give rise to an angular spread in the photon beam

$$\sigma_{\theta\gamma} \approx \frac{3.1}{E} \text{ mr}, \tag{15}$$

with E the beam energy in GeV. In the worst case at 3 GeV, the angular spread $\sim$ 1 mr. Both this and the size of the photon beam (of order 1 mm or less) will contribute to the overall angular resolution of the experiment, as discussed in detail in Sec. III F. Other photon experiments proposed for Halls A and C utilize a mixed photon and electron beam by transporting the electron beam from the radiator through the target, and on to the beam dump. It then becomes necessary to remove the electron-induced background by doing a subtraction of the yield obtained with the radiator removed. This greatly simplifies the beam-handling situation, since no extraordinary techniques are needed to dump the electron beam cleanly before it hits the scattering target. In the present experiment, the electron-induced background due to ep scattering may be too severe to allow this technique to be used. In effect, the kinematics of ep elastic scattering at these energies is identical to that of γp elastic scattering for a bremsstrahlung photon at the endpoint of the spectrum. This requires a very efficient electron veto in the photon arm. However, there is an additional background due to the fact that the scattered electron may radiate a hard photon via either internal or external bremsstrahlung. The radiated photon from $ep\gamma$ essentially maintains the direction of the electron, so that this process becomes indistinguishable from Compton scattering. Since most of the electrons incident on the hydrogen target have an energy very close to the initial beam energy, the $ep\gamma$ background is reduced considerably by selecting events in the recoil spectrometer corresponding to incident photon energies below the bremsstrahlung endpoint by an amount we denote by ϵ. In Sec. III G, we will show that this background can be reduced to an acceptable level with $\epsilon \approx 0.1$ GeV, i.e., by eliminating events in the upper 0.1 GeV of the bremsstrahlung spectrum.

One addition remark is in order. There will be many Möller electrons from the radiator, and since the Möller cone is $\sim$ 10 mr, some electrons may scatter into the downstream beam pipe at the exit to the scattering chamber, creating an unacceptable background. Therefore it may prove necessary to move the radiator closer to the target and/or modify the exit port of the scattering chamber to increase the size of the aperture. This issue is currently under study and a final resolution must await tests with a radiator in the beam, which will be performed in the next few months (see Sec. V).

C. Proton Arm

The important acceptance parameters for present purposes are follows: momentum acceptance of $\pm 4.5\%$; angular acceptance of 51 mr and 102 mr in the horizontal and vertical planes, respectively; transverse length (y) acceptance of $\pm$ 3 cm; and maximum central momentum of 4.5 GeV (for the HRS currently used in the electron arm). These parameters have already been achieved. The important resolution parameters are the horizontal angle (σ_θ), the vertical angle (σ_ϕ), and the transverse target (σ_y). The best information available on the angular resolutions comes from an *ep* scattering run at 4 GeV beam energy, where a missing momentum resolution σ_{pm}=4 MeV/c was measured for the combined spectrometers (see Fig 8). The proton and electron each had a momentum of 2.5 GeV and the angles were approximately 30° for each spectrometer. The measured resolution includes effects of multiple scattering, which should be relatively small at these energies. Assuming equal contribtions from each spectrometer and from each of the horizontal and vertical angles, we find $\sigma_\theta \approx \sigma_\phi \approx 0.9$ mr. This is quite good and comparable to the design goals for the vertical angle, although still a factor of two larger than the design goal for the horizontal angle. The best information available on the y-resolution comes from the recent $^{16}O(e,e'p)$ experiment, in which the detected electron at 2 GeV in the HRS had $\sigma_y \approx 0.9$ mm (see Fig. 9). This is somewhat worse than the design goal but still quite good. In the estimates to follow, we will assume that these results will continue to be achievable.

The combined angular and momentum acceptance of the HRS determines the range of photon energies that are accepted. In fact, this range is probably too large for all of the kinematics of interest to us. After eliminating the upper 0.1 GeV of the bremsstrahlung spectum as discussed above, we intend to restrict the measurement to an energy fraction $\Delta E_\gamma / E_\gamma = 10\%$. This will help reduce any uncertainty due to nonelastic contributions to the scattering cross section. This is further discussed in Sec. III H.

D. Target

The target will be the standard Hall A LH_2 target. We assume a target cell 15 cm long and 6.35 cm in diameter, with a 0.07 mmm Al entrance window and 0.18 mm Al side walls. The target is contained in the Hall A scattering chamber, which will soon have an Al exit window of thickness 0.25 mm. These numbers will enter into the multiple scattering calculation that determines the overall angular resolution.

E. Photon Arm

The key new piece of instrumentation for this experiment is a calorimeter made of Pb-Glass blocks that will be used to detect the scattered photon. We use Pb-Glass rather than alternatives based on scintillators or wire chambers in order to minimize the sensitivity to hadronic background. We assume an array of 4 cm x 4 cm x 40 cm blocks of type F8 or similar variety. These will be arranged in 25 x 25 array for a total of 1 m x 1m. This array satisfies the essential requirements, which we now discuss

The solid angle should be reasonably matched to the acceptance of the proton arm. In the vertical plane, the acceptance required is

$$\Delta\phi_\gamma = \frac{sin\theta_\gamma}{sin\theta_p}\Delta\theta_p = \pm\frac{sin\theta_\gamma}{sin\theta_p}[25\text{mr}] \tag{16}$$

This relation follows from the coplanarity condition on the proton and photon. Since large photon angles θ_γ are correlated with small recoil proton angles the required vertical acceptance $\Delta\phi_\gamma$ grows very large at large angles. The horizontal acceptance is more complicated, since it depends on both the angular $\Delta\theta_p$ and momentum Δp_p acceptance of the proton spectometer, as well as on the limitations imposed by the $\Delta E_\gamma/E_\gamma = 10\%$ condition. We have calculated the necessary acceptance in both ϕ_γ and θ_γ for all the kinematics of the experiment. The results for the 5 GeV kinematics (for which the angular range is greatest) are shown in Fig. 10. We see that the required $\Delta\theta_\gamma$ also grows large at large scattering angles, although not as rapidly as the required $\Delta\phi_\gamma$. Our detector will have an angular acceptance that can be adjusted at each scattering angle to match the horizontal angular acceptance (see Table I). We can do this for all but the most backward angle (135° at 5 GeV), since it is not desirable to have the calorimeter closer than 5 m from the target. Moreover, for most of the backward angles, $\Delta\phi_\gamma$ will be somewhat lower than optimal. The movement will be achieved by mounting the detector on a carriage that allows both rotation about the target position but also radial movement.

Sufficient segmentation is needed to maintain the good angular resolution necessary for reduction of the π^0 background. Since the Moliere radius of Pb-Glass is 3.3 cm, the 4 cm square blocks are a good choice. We should have no problem achieving a position resolution $\sigma_x = 5$ mm with such detectors [21]. The experience of the Yerevan group is that the position resolution for similar detectors is approximately

$$\sigma_x = \frac{5\,mm}{\sqrt{E}},$$

which is more than sufficient for our purposes. In our estimates of the π^0 background to be given in Sec.III F, we will assume the more modest number of 5 mm. The ability to calibrate accurately with an electron beam (see Sec. III K) should allow us not only to measure σ_x accurately but also to develop optimization algorithms for achieving the best position resolution possible [21].

Since we will primarily use angular kinematics to identify Compton events, only modest energy resolution is needed. The BNL group [21] reports an energy resolution

$$\sigma_E = .06\sqrt{E} + .02E, \tag{17}$$

which should suffice for our purposes.

For data acquisition, the standard Hall A DAQ will be used with the addition of two Fastbus crates with the calorimeter electronics. Based on recent experience in both Hall A and Hall C, the singles rate in the proton arm will be low enough to serve as the primary trigger. In a recent Hall C experiment with a 4 GeV electron beam on a 15-cm LH_2 target in kinematics very similar to ours, the single-arm trigger rate in the HMS was 150 Hz at 10 μA. We estimate that the presence of the radiator will increase this by a factor of 5, bringing the total trigger rate to less than 1 kHz.

F. Background from π^0 Photons

The goal is to separate the $p(\gamma,\gamma' p)$ events from the $p(\gamma,\pi^0 p)$ events. Because of the small mass of the pion, the four-momentum of a coherently produced π^0 is nearly identical to that of a Compton photon. For a monochromatic incident photon beam, it would be possible to resolve Compton from π^0 events by a precise measurement of the three-momentum of the recoil proton (indeed, this is essentially the technique used in the VCS experiments), but this will not work for a continuous bremsstrahlung spectrum. Instead one relies on the kinematic correlation between the recoil proton and the associated Compton photon or π^0 . Under the assumption of two-body kinematics, a measurement of the three-momentum of the recoil proton uniquely defines both the energy of the photon that initiated the event and the three-momentum of the photon or π^0 . The π^0 decays into two photons. The higher energy photon has an energy between $E_\pi/2$ and $E_\pi \approx E'_\gamma$ (the energy of a scattered photon in the same kinematics) and is confined to a cone of half-angle m_π/E_π about the pion direction. The lower energy photon has an energy less than $E_\pi/2$ and lies outside the cone. In contrast, for fixed kinematics of the recoil, the Compton photon is spread out in solid angle only by the overall angular resolution of the coincidence detection system. This resolution is determined by the intrinsic resolution of the magnetic spectrometer for the in-plane and out-of-plane proton angles and for vertex reconstruction; by proton multiple scattering in the target and other material; by the angular spread of the incident photon beam; and by and the ability of the calorimeter to determine the angle of the scattered photon. We combine all these effects into effective Compton angular resolutions, which we denote by σ_θ and σ_ϕ for the horizontal and vertical directions, respectively. The ratio R_{π^0} of coherent π^0 photons to Compton photons is therefore determined by the ratio of cross sections divided by the fraction of the π^0 photons falling within the angular resolution. One easily finds

$$R_{\pi^0} = 11 \frac{d\sigma(\gamma,\pi^0)}{d\sigma(\gamma,\gamma)} \frac{\sigma_\theta \sigma_\phi}{(m_\pi/E'_\gamma)^2}, \tag{18}$$

where the numerical factor comes in part from the fraction of Compton events within 2σ of a two-dimensional Gaussian distribution.

We see then that the Compton and π^0 events are distinguished by the distributions of $\delta\theta_\gamma$ and $\delta\phi_\gamma$ which are, respectively, the difference of the measured in-plane and out-of-plane photon angles and the reconstructed photon angle based on the measurement of the proton kinematics measured in the HRS. The resolutions in these quantities, σ_θ and σ_ϕ, respectively, directly enter into the expression for R_{π^0} given above. Typical histograms of these quantities generated by Monte Carlo are shown in Fig. 11. It is important to note that enough of the π^0 photon distribution can be measured in the experiment to extrapolate the distribution accurately under the Compton peak. Therefore, the running time needed to obtain a given statistical precision in the measurement of the Compton cross section is proportional to $1+R_{\pi^0}$. We now present a detailed discussion of the calculation of R_{π^0} for the one case in our proposed kinematics, namely for 6 GeV at 110°. The quantity σ_ϕ has contributions from the following:

- σ_x^γ, the position resolution of the calorimeter. We assume this to be 5 mm, as discussed

earlier. At a distance of 6 m (determined by the horizontal angular acceptance), this contributes 0.8 mr to σ_ϕ.

- σ_ϕ^p, the out-of-plane angular resolution of the HRS. We assume the value 0.9 that has been achieved already, leading to a contribution to σ_ϕ of 1.8 mr.
- The proton multiple scattering in the target. This is calculated using standard formulas, taking into account the hydrogen in the target, the aluminum wall of the target can, and the exit aluminum foil to the scattering chamber. Together these contribute 0.8 mr.
- The vertical angular spread of the photon beam. This is calculated assuming it is due to multiple scattering by the electron beam in the radiator. It contributes 1.0 mr.
- The vertical beam spot size. We calculate this by assuming the spot size is due to the angular spread and therefore less than 1 mm. It contributes 0.8 mr.

Similarly, σ_θ has contributions from the following:

- σ_x^γ, the position resolution of the calorimeter. Once again, this contributes 0.8 mr.
- σ_θ^p, the in-plane angular resolution of the HRS. We again use the value 0.9 mr that has already been achieved, leading to a contribution of 3.3 mr.
- the proton multiple scattering in the target. This contributes 1.4 mr.
- The horizontal angular spread of the photon beam. This contributes 1.0 mr.
- The horizontal beam spot size. This contributes 0.1 mr.
- σ_y^p, the resolution in proton vertex reconstruction along the beam line. We use the value 0.9 mm that has been achieved, leading to a contribution of 0.3 mr.
- σ_p, the proton momentum resolution. This contributes negligibly.

Combining these independent contributions in quadrature, we find σ_θ=3.8 mr and σ_ϕ=2.5 mr. By comparison, the Cornell experiment achieved 8.5 in θ and 2.1 in ϕ. The above number show that these results are dominated by contributions from the HRS, σ_θ^p and σ_ϕ^p, so that is where any improvements should be aimed. The resolutions calculated for all our proposed kinematics are given in Table II.

To calculate R_{π^0} , we use scaling law estimates which roughly fit the Cornell data for both the $p(\gamma,\gamma' p)$ cross section

$$\frac{d\sigma(\gamma,\gamma)}{dt} = \frac{30\,\mu b\,GeV^{10}}{s^6}, \tag{19}$$

and the $p(\gamma,\pi^0 p)$ cross section

$$\frac{d\sigma(\gamma,\pi^0)}{dt} = \frac{20\,mb\,GeV^{12}}{s^7}. \tag{20}$$

In Table II, we see that $R_{\pi^0} \approx$ 1.2-1.4, essentially independent of our kinematics. The worse angular resolution at backward angles (as the detector moves closer to the target) is compensated by the larger π^0 cone.

G. Background from e-p Scattering

As discussed above, the presence of electrons in the beam introduce two types of coincidence background that are kinematically indistinguishable from Compton scattering. The first is simply elastic ep scattering, where the scattered electron is detected in the calorimeter. The second is ep scattering followed by emission of a hard bremsstrahlung photon in the direction of the scattered electron, which we refer to as an $ep\gamma$ event. As remarked earlier, since most of the electrons in the beam are right at the bremsstrahlung endpoint, we eliminate much of the problem by tuning the spectometer to accept events corresponding to incident photons in the range E_γ^{min} to E_γ^{max}, where E_γ^{max} is approximately 0.1 GeV from the endpoint. We further assume $E_\gamma^{max}/E_\gamma^{min} \approx 1.1$. It is now straightforward to estimate the scope of the problem. To do this, we use the Matthews and Owens bremsstrahlung spectrum [22] to count the relative numbers of bremsstrahlung photons and post-bremsstrahlung electrons in the interval between $E_\gamma^{min} - E_\gamma^{max}$, and use the Rosenbluth cross section for ep scattering and the expression of Eq. 19 for the Compton cross section. This actually overestimates the problem at forward angles, since the ep cross section rises steeply whereas Eq. 19 is flat, whereas the Cornell cross sections also rise steeply at center of mass angles forward of 90° (see Ref. [2]). A more realistic procedure is to use Eq. 19 for $\theta_{cm} \geq 90°$ and the expression

$$\frac{d\sigma(\gamma,\gamma)}{dt} = \frac{30\,\mu b\,GeV^{10}}{s^6\,(1-\cos\theta_{cm})^4}, \tag{21}$$

for $\theta_{cm} \leq 90°$. We have calculated the ratio of scattered electons to photon $N_{ep}/N_{\gamma p}$ for the proposed kinematics. That ratio ranges from a few at the backward angles to a few hundred at the forward angles. It is clear that we need to reject electrons at the level of about 1 part in 1000 in order to keep the ep background at a reasonable level. Before discussing this, we first estimate the $ep\gamma$ problem by calculating the probability that the scattered electron will radiate a photon in the energy range $E_\gamma^{min} - E_\gamma^{max}$, including both the external and internal bremsstrahlung. Using a Monte Carlo calculation and including the effects of detector resolution, we find that at 6 GeV the ratio of $ep\gamma$ to Compton events is approximately 20% at 70°, 10% at 90° and 6% at 110°. Sample histograms for the 6 GeV 70° and 110° points are shown in Fig. 12 and 13, respectively. We remark that this is one case where it would be beneficial to have good energy resolution in the calorimeter, since the bremsstrahlung background steeply rises at low energy, whereas the Compton photons are concentrated at high energy. It will be necessary to measure this background in order to subtract it. We can do this straightforwardly through the calibration procedure described in Sec. III K.

We turn now to the ep background. We attack this problem in two ways. First, we use a magnet to deflect electrons in order to remove the kinematic correlation with the recoil proton. A modest field integral of 0.1 T-m as close as possible to the target will bend a 3 GeV electron 10 mr, deflecting the electron by at least 4 cm (assuming a magnet-to-calorimeter distance of at least 4 m), which is more than sufficient to remove the correlation. Moreover, charged particles with momentum less than 0.3 GeV will be deflected completely off the face of the calorimeter, thereby reducing the total flux impinging on the detector. A vertical field will be used to take advantage of the small vertical size of the photon beam. The overall size of the field region will be about 50 cm, with a 30 cm gap.

Second, we use a veto detector to reject electon-induced events in the calorimeter. In an upcoming test run scheduled for the beginning of March, we will investigate various schemes for rejecting electrons, including a MWPC, an air Cerenkov detector, and plastic scintillators. Whichever technique is used, sufficient segmentation needs to be arranged in view of the high rate of electron background expected (up to 1 MHz). The excellent position resolution of the calorimeter suggests using a position- sensitive veto technique. A MWPC provides 2 mm position resolution with a simple and reliable readout system. With 150 ns time resolution, a rate $\sim 10^5$ Hz per cell will be acceptable. With a combined resolution of MWPC and calorimeter of $\sim$3 mm, a cell size of $\sim$ 2x2 cm can be used in the off-line veto analysis. A segmented gas Cerenkov counter is an attractive possibility because of the ability to adjust the threshold and because the directionality of Cerenkov radiation will made this counter sensitive to the electrons coming from the target area. For an electron energy threshold of $\sim$ 30 MeV and a counter length of 3 m, an efficiency above 99.9% might be possible. Arrays of plastic scintillator counters would have $\sim$ 1 cm postion resolution and $\sim$ 10 MeV threshold for detection of the charged particles. A decision as to which method will be used in the actual experiment must await further tests. Nevertheless, the collaboration is confident that the electron problem is under control.

H. Other Backgrounds

If one is within one pion mass from the bremsstrahlung endpoint, then no other process is possible other than elastic scattering and π^0 photoproduction. However, in the present experiment, we will use incident photons as much as 0.7 GeV below the endpoint (in the case of a 6 GeV beam. The important point is that any $\geq$ 3-body final state will not have a kinematic correlation between the recoil proton and the detected photon. For example, consider the case of η photoproduction followed by decay to two photons. The kinematics for this process is similar to the π^0 case except that the η is four times more massive, so that the decay cone is 16 times wider. This would give rise to a smooth background under the π^0 cone, which includes the Compton events, so that the good angular resolution discriminates against such background. As another example, consider inelastic photon scattering leaving the proton in an excited state, which then decays into a proton and pion. Once again, the smearing of the kinematics due to the momentum of the third particle (in this case, the pion) gives rise to a cone roughly centered on the Compton kinematics. For the specific case of scattering into the Δ resonance, the decay cone is about 50% larger than the π^0 cone. In investigating whether such a background exists, it is useful to have sufficient angular acceptance to look outside the π^0 cone for the presence of a smooth background that can be extrapolated into the region of interest and subtracted. This procedure was followed in the Cornell experiment, where very little background was found [2]. We will follow a similar procedure in the proposed measurements.

I. Luminosity Considerations

We now address the issue of luminosity limitations imposed by the counting rates in the photon arm. To this end, our approach has been to do measurements in some limited

kinematic range and then use a Monte Carlo code to extrapolate into other regions. The code we have used was designed for radiation shielding calculations and uses the DINREG event generator in the framework of GEANT detector simulations and particle transport code. In order to test this code and gain some experience with unshielded calorimeters in an electron-scattering environment, we used 1 shift of beam time during July 1997 to do a series of measurements with an array of 9 blocks, each of dimension 6 cm by 6 cm by 74 cm. A 2.4 GeV electron beam was used with a waterfall target of thickness 0.5 g/cm^2 (1.4% radiation length). The calorimeter array was set at 41° with respect to the beam at a distance of 5 m from the target, subtending a total solid angle of 1.3 msr. At this angle, scattered electrons have an energy of 1.5 GeV. With a beam intensity of 10 μA, the summed counting rate in the calorimeter was 9.5 kHz above a threshold of 0.5 GeV and 2.1 kHz above 1.0 GeV. The Monte Carlo predicted about 10±2 kHz of electrons plus photons above 0.50 GeV, which is remarkably consistent with the measurement.

With the Monte Carlo code reasonably calibrated, we now use it to extrapolate to kinematics and luminosities of interest for the Compton experiment, for which we will use a copper radiator of thickness 0.8 g/cm^2 (6% radiation length), a scattering target of 1 g/cm^2 Hydrogen, and a beam of intensity 10 μA. The worst case situation is the 6 GeV point at $\theta_{cm} = 70°$, for which the calorimeter is at $\theta_{lab} \sim 20°$ and the scattered photons/electrons have an energy of 4.3 GeV. Assuming a 1 m^2 detector at 15 m (which matches the HRS acceptance), the code predicts a total rate (electrons plus photons) of 4 MHz above 0.5 GeV or 0.5 MHz above 2 GeV (see Figs. 14 & 15)

It is worth noting that the Monte Carlo tells us that there is very little direct electron or photon background in the calorimeter from the radiator. Instead, the principal background comes from photons from the radiator interacting with the Hydrogen target. This suggests that it might be possible to locate the radiator just before the entrance window of the target cell, as discussed above in Sec. III B.

J. Counting Rate Estimates

The counting rate is given by

$$\frac{dN_{\gamma\gamma}}{dt} = TX\left[\frac{I}{e}\right]\frac{d\sigma}{d\Omega_p}\frac{\Delta E_\gamma \Delta\Omega_p}{\bar{E}_\gamma}, \tag{22}$$

where T is the target thickness, X is the radiator thickness, I is the beam current, $-e$ is the electron charge, $\bar{E}_\gamma$ is the mean incident photon energy over the acceptance interval ΔE_γ, and $\Delta\Omega_p$ is the angular acceptance of the proton spectrometer. Rate estimates in counts/hour are given in Table II. These estimates assume a 15-cm long liquid Hydrogen target ($T = 6.3 \times 10^{23}\, cm^{-2}$), a 6% radiator ($X = 0.06$), a modest beam current of 10 μA, and the HRS parameters discussed above. The calculation of the rates takes into account the geometrical acceptance of the calorimeter, which is largely matched to the acceptance in the proton arm in the horizontal plane but not in the vertical (see Sec. III E). Further, we assume the Compton scattering cross section is given by Eq. 19. Note that the Cornell data suggest that this formula underestimates the Compton cross section as scattering angles forward of $\theta_{cm} = 90°$. Also shown in Table II are the expected background due to the π^0 photons.

K. Systematic Errors

Our goal is to measure the Compton scattering cross section to a statistical precision of 5% and with overall systematic uncertainty on the order of 6%. We arrive at this number from the sum in quadrature of four nearly identical contributions of 3% each: the HRS acceptance (including all effects associated with electron beam monitoring, target thickness, data acquisition deadtime, etc.), the shape and intensity of the bremsstrahlung flux, the acceptance of the calorimeter, and the $ep\gamma$ background subtraction. ¿From recent experiments in Hall A, cross sections have already been measured to an absolute accuracy of 5%. We assume that as additional experience is gained over the next few years, this accuracy will be improved to about 3% Our estimate for the uncertainty due to the bremsstrahlung flux comes from experience with other experiments using mixed photon/electron beams (such as E89-012 or SLAC NE17). The calorimeter acceptance will be measured with ep elastic scattering, so it too will be known on the order of 3%. The calibration procedure is described below. The $ep\gamma$ background has been discussed above. The background is expected to be at worst 20% of the Compton signal, except for the 5 GeV, 60° point, and it will be measured in our calibration procedure, described in the next paragraph. A calibration on the order of 15% therefore reduces the systematic error to at worst 3%. If our estimate of the $ep\gamma$ turns out to be too low, then we will have to settle for somewhat worse systematic errors for the forward angles. The principal effect of these systematic errors will be an uncertainty in the overall cross section scale. Point-to-point systematic errors will be minimized by using the 2nd HRS spectrometer as a luminosity monitor.

A nice feature of our setup is that we can use elastic ep scattering to do an energy calibration of the calorimeter, measure the angular placement and acceptance, and measure the position resolution. This is done with the radiator removed and the sweep magnet turned off. With the radiator still removed but the sweep magnet turned on, we can measure the radiation probability in order to make the $ep\gamma$ correction. With the radiator in, the sweep magnet off, and the spectometer tuned for a momentum below the elastic peak of the primary beam, we will measure the spectrum of energy-degraded scattered electons in the calorimeter, which again will be important for the $ep\gamma$ correction. It is likely that such measurements will have to be done for each kinematic setting

IV. BEAM REQUEST AND RUN PLAN

A. Beam Request

The parameters of the measurements we propose are presented in Tables I and II. The last column of Table II gives the time needed to achieve 5% statistics for the Compton cross section, including the effect of the (modest) π^0 background. These times total about 65 hours. This represents about 1/3 of the total running time needed for the experiment. The remainder of the time will be needed for calibrations with the electron beam and measurements with the radiator removed. At the most forward angles, it may also be

necessary to measure with an empty target, although the excellent y-resolution of the HRS should allow us to separate events from the Al entrance window. There is also overhead associated with energy and angle changes, which we budget at approximately 2 hours per change, for a total of 32 additional hours. Therefore, our total beam request is 227 hours.

V. COLLABORATION RESPONSIBILITIES AND TIMETABLE

The organization of the RCS collaboration is rather new, but specific responsibilities of the various groups have been explored in a preliminary way. The collaboration includes a broad range of experience and expertise involving every phase of the experiment, including operation of the Hall A spectrometers, cryotarget, and beam lines; use of real photon beams and mixed photon/electron beams to study photoreactions; design and construction of large, multi-element Pb-Glass calorimeters; optimization of position resolution in electromagnetic calorimeters; construction and use of a variety of veto dectectors, such as MWPC, Cerenkov, and plastic scintillators; mechanical design of detector carriages; design and use of sweep magnets; data acquisition and trigger electronics; and data analysis. A major segment of the collaboration works together on the VCS experiments. Another segment has done considerable work on Compton scattering from the proton at lower energies. By late February, we expect to have an organizational collaboration meeting, during which working subgroups will be formed to address the various experimental issues associated with this experiment.

Test runs are planned in March and June of 1998 during which we will set up an 5 x 5 array of candidate Pb-Glass blocks (provided by the Yerevan group) in coincidence with the hadron HRS. Using electron scattering from the Hydrogen target, we will develop off-line techniques for optimizing the position resolution of the calorimeter. We further intend to study 3 different schemes

- Test of a 5 x 5 array of candidate Pb-Glass blocks, including studies of algorithms for optimizing the position resolution
- Test of various schemes to veto electrons from *ep* scattering.
- Test of luminosity limitations imposed by a radiator.

VI. FUTURE DEVELOPMENTS

In thinking about Compton scattering in this energy regime, it would be very attractive to measure double polarization observeables. As we gain experience with unpolarized measurements, we see the development of a full proposal as a future direction. Two types of experiments are possible. Both would use longitudinally polarized electrons. One would measure the recoil polarization using the FPP in Hall A. The second would use a polarized target in Hall B. A second option for the future would try to take advantage of future energy upgrades to extend the unpolarized measurements to 8 GeV and beyond. To take full advantage of the higher momentum transfer afforded by higher energy beams, it will be advantageous to move the experiment to Hall C and detect the recoil proton in the HMS.

TABLES

TABLE I. Kinemates for the proposed RCS measurements. E is the beam energy and $\bar{E}_\gamma$ is the mean photon energy in a 10% interval whose maximum energy is 0.1 GeV below E. D is the target-to-calorimeter distance needed to match the HRS acceptance.

E (GeV)	$\bar{E}_\gamma$ (GeV)	s $(GeV)^2$	θ_{cm} (deg)	$-t$ (GeV^2)	D (m)	θ_γ (deg)	E'_γ (GeV)	θ_p (deg)	p_p (GeV)	$p_\perp$ (GeV)
3.00	2.77	6.08	90.	2.22	9.	41.7	1.58	33.6	1.90	1.05
3.00	2.77	6.08	110.	2.98	6.	57.1	1.18	25.0	2.35	0.99
4.00	3.72	7.87	90.	3.10	9.	37.0	2.07	31.0	2.42	1.25
4.00	3.72	7.87	110.	4.16	6.	51.1	1.50	22.8	3.01	1.17
5.00	4.68	9.66	60.	1.99	17.	19.8	3.61	43.8	1.77	1.22
5.00	4.68	9.66	70.	2.62	14.	23.9	3.28	38.3	2.14	1.33
5.00	4.68	9.66	80.	3.30	11.	28.4	2.92	33.4	2.53	1.39
5.00	4.68	9.66	90.	3.99	9.	33.6	2.55	29.0	2.92	1.41
5.00	4.68	9.66	100.	4.68	8.	39.6	2.18	24.9	3.30	1.39
5.00	4.68	9.66	110.	5.35	6.	46.7	1.82	21.2	3.67	1.33
5.00	4.68	9.66	120.	5.98	5.	55.2	1.49	17.7	4.02	1.22
5.00	4.68	9.66	135.	6.81	5.	72.2	1.05	12.9	4.47	1.00
6.00	5.63	11.45	70.	3.21	14.	22.0	3.92	36.3	2.48	1.47
6.00	5.63	11.45	80.	4.03	11.	26.2	3.48	31.5	2.94	1.54
6.00	5.63	11.45	90.	4.88	9.	31.0	3.03	27.2	3.41	1.56
6.00	5.63	11.45	100.	5.72	8.	36.6	2.58	23.4	3.88	1.54
6.00	5.63	11.45	110.	6.55	6.	43.2	2.14	19.8	4.33	1.47

TABLE II. Counting rates and backgrounds for the proposed measurements. The angular resolution is given in columns 4 and 5. The yield of Compton events is given in column 6. The ratio of π^0 to Compton events is given in column 7 and the projected time to achieve 5% statistics for Compton events is in the last column.

E	$\bar{E}_\gamma$	θ_{cm}	σ_θ	σ_ϕ	$Y_{\gamma\gamma}$	R_{π^0}	T
(GeV)	(GeV)	(deg)	(mr)	(mr)	counts/hr		hr
3.00	2.77	90.	3.5	2.3	2202.	1.26	0.4
3.00	2.77	110.	4.2	3.3	3813.	1.21	0.2
4.00	3.72	90.	3.2	1.9	792.	1.25	1.1
4.00	3.72	110.	4.0	2.9	1334.	1.24	0.7
5.00	4.68	60.	2.8	1.0	108.	1.38	8.9
5.00	4.68	70.	2.8	1.1	166.	1.32	5.6
5.00	4.68	80.	2.9	1.4	250.	1.30	3.7
5.00	4.68	90.	3.1	1.7	350.	1.30	2.6
5.00	4.68	100.	3.4	2.1	424.	1.29	2.2
5.00	4.68	110.	3.9	2.6	553.	1.31	1.7
5.00	4.68	120.	4.5	3.4	587.	1.32	1.6
5.00	4.68	135.	6.0	5.1	386.	1.30	2.4
6.00	5.63	70.	2.6	1.0	80.	1.35	1.8
6.00	5.63	80.	2.8	1.2	123.	1.36	7.7
6.00	5.63	90.	3.0	1.5	177.	1.38	5.4
6.00	5.63	100.	3.3	1.9	215.	1.38	4.4
6.00	5.63	110.	3.8	2.5	265.	1.41	3.6

REFERENCES

[1] T.H. Bauer, *et al.*, Rev Mod Phys **50** (1978) 261.

[2] M.A. Shupe *et al.*, Phys Rev **D19**, 1929 (1979).
[3] S.J. Brodsky and G. Farrar, Phys. Rev. Lett. **31** (1973) 1953.
[4] Glennys R. Farrar and Huayi Zhang, Phys Rev Lett **65**, (1990) 1721,
Glennys R. Farrar and Huayi Zhang, Phys Rev **D41** (1990) 3348, and
E. Maina and G.R. Farrar, Phys Lett **B206** (1988) 120.
[5] A.S. Kronfeld and B. Nizic, Phys Rev **D44** (1991) 3445.
[6] H.N. Li and G. Sterman, Nucl Phys **B381**, 129 (1992).
[7] A. Radyushkin, in **Baryons-92**, M. Gai ed., World Scientific, (1993) p. 366,
[8] J. Bolz and P. Kroll, Z Phys **A356**, 327 (1996)
[9] P. Kroll, M. Schürmann and W. Schweiger, Nucl. Phys. Int. J. Mod. Phys. **A6**, 4107 (1991).
[10] P. Kroll, M. Schürmann, and P.A.M. Guichon, Nucl Phys **A598**, 435 (1996).
[11] R.P. Feynman, **Photon-Hadron Interaction**, W.A. Benjamin, Reading MA, 1972.
[12] C. Corianò, A. Radyushkin, G. Sterman, Nucl Phys **B405**, 481 (1993), and C. Corianò and H. Li, Phys Lett **B324**, 98 (1994).
[13] X. Ji, Phys Rev Lett **78**, 610 (1997), and
X. Ji, Phys Rev **D55**, 7114 (1997)
[14] A.V. Radyushkin, Phys Lett **B380** (1996) 417.
[15] A.V. Radyushkin, private communication, 1997.
[16] P.A.M.Guichon and M. Vanderhaeghen, Progress in Nuclear Physics **41** (1998) in press.
[17] M. Vanderhaeghen, P.A.M Guichon and J. Van de Wiele, Nucl Phys **A622**, 144c (1997).
[18] I.D. King and C.T.Sachrajda, Nucl Phys **A598**, 785 (1987)
[19] V.L. Chernyak, A.A. Oglobin, and A.R. Zhitnitsky, Z Phys **C42**, 569 (1989).
[20] V.L. Chernyak and A.R. Zhitnitsky, Phys Rep **112**, 173 (1984).
[21] R. R. Crittenden, *et al.*, Nucl. Instr. and Meth. A **387**, 377 (1997).
[22] J. L. Matthews and R. O. Owens, Nucl. Instr. and Meth. **111**, 157 (1973).

FIGURES

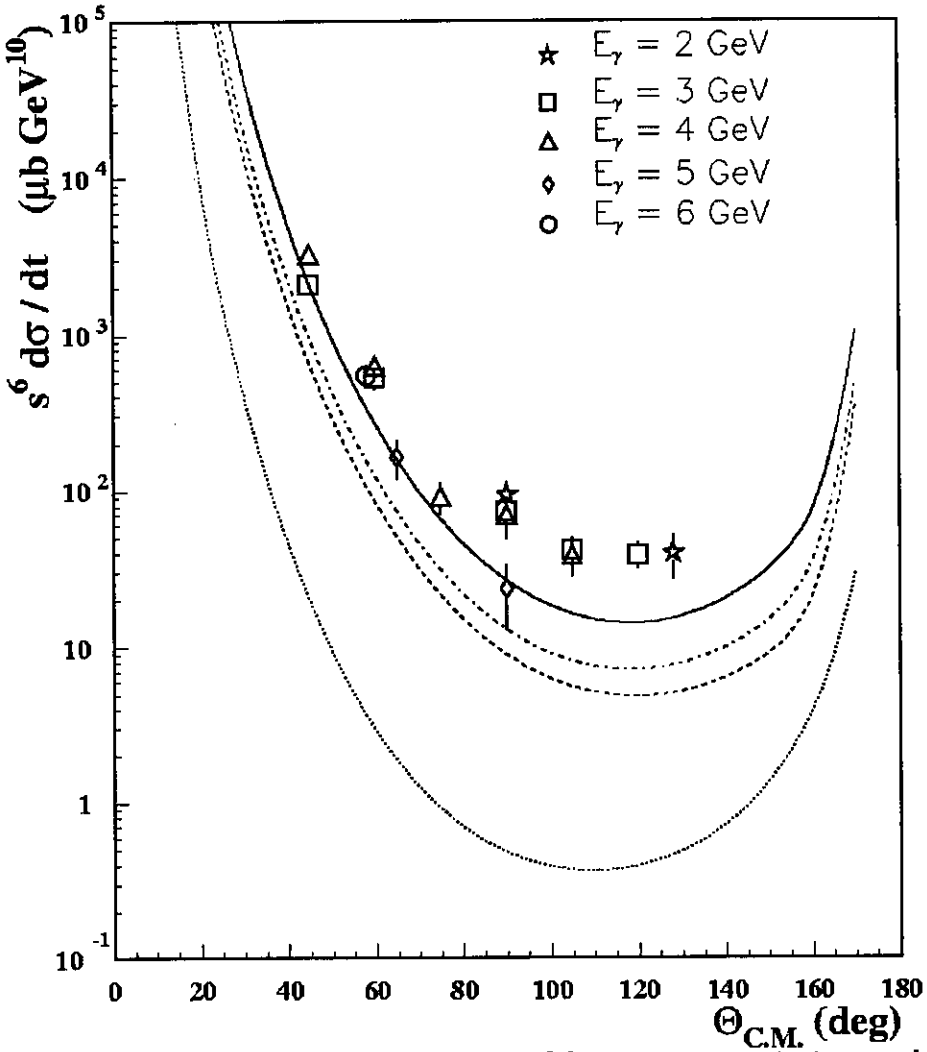

FIG. 1. Real Compton scattering data of Shupe [2] and pQCD calculations [5,16,17] using various distribution amplitudes ϕ for the proton structure. Solid line: KS [18], dot-dashed line: COZ [19], dashed: CZ [20], and dotted: asymptotic DA.

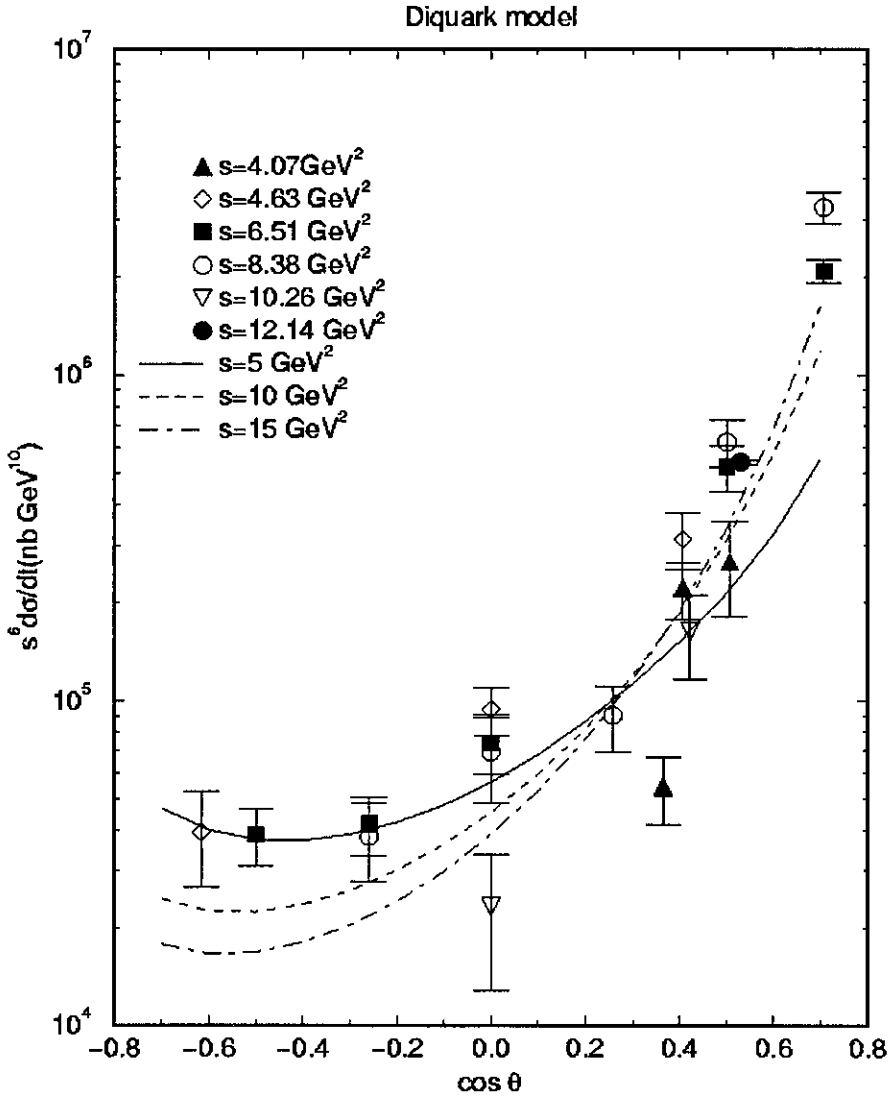

FIG. 2. Real Compton scattering data of Shupe [2] and the di-quark model calculations at various values of the center of mass energy squared s. [9,10,16]

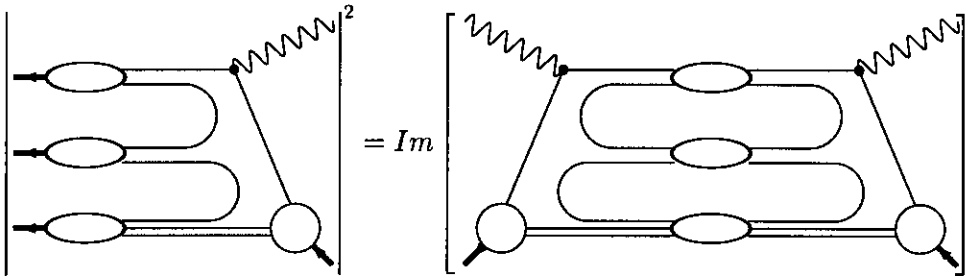

FIG. 3. The photo-absorption cross section and the imaginary part of the forward Compton amplitude for real or virtual photons. The figures are drawn from right to left in the form of a matrix element $\langle f | \mathcal{M} | i \rangle$. The figure illustrates schematically the sum over all hadronic states in the final state of photo-absorption or the intermediate state of Compton scattering.

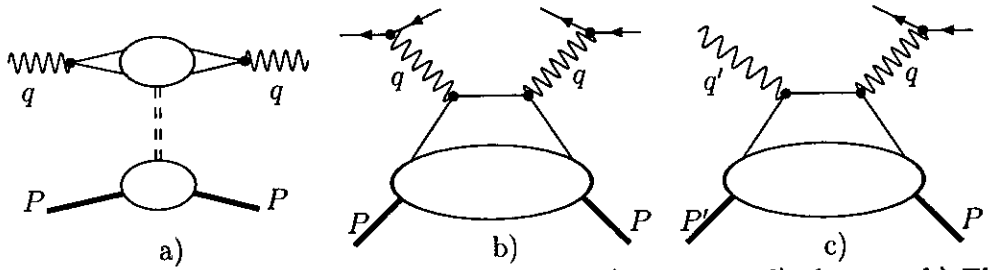

FIG. 4. a) The forward Compton amplitude for real (or quasi-real) photons. b) The handbag diagram for the forward virtual Compton amplitude measured in deep inelastic lepton scattering. c) The leading twist contribution to the "off-forward" or deeply virtual Compton scattering (DVCS) amplitude: VCS in the limit $Q^2 = -q^2$ large, $q'^2 = 0$, and $-t = (q-q')^2 = (P'-P)^2 \ll Q^2$. Fig. a) illustrates the dominance of t-channel hadronic exchange for forward (real) Compton scattering. Figs. b) and c) illustrate factorization at high Q^2 for b) DIS and c) forward VCS. [13,14]

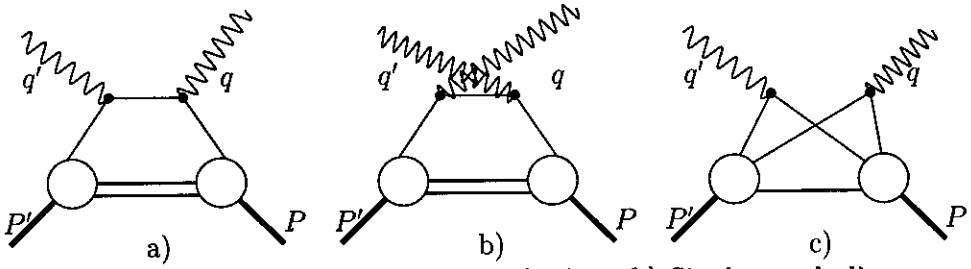

FIG. 5. Compton amplitude in hard scattering limit. a,b) Single-quark diagram: a) direct or s-channel term, b) crossed or u-channel term. c) Two-quark diagram. These diagrams can be dressed with perturbative gluon exchanges.

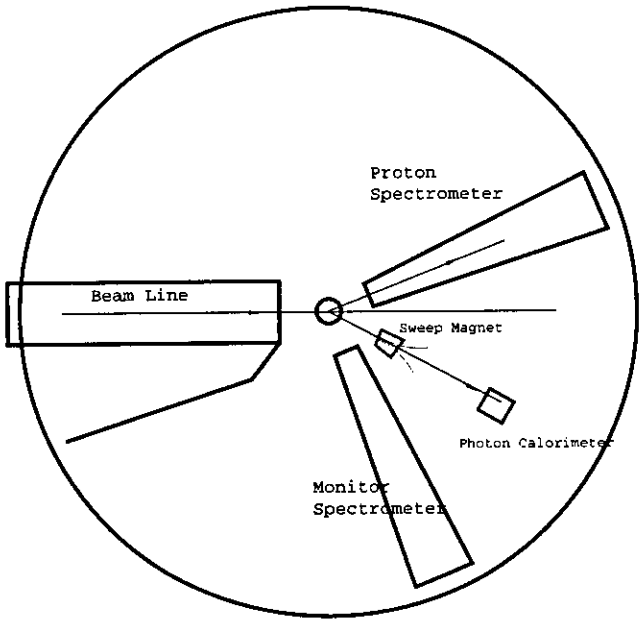

FIG. 6. Plan view of the proposed experiment in Hall A

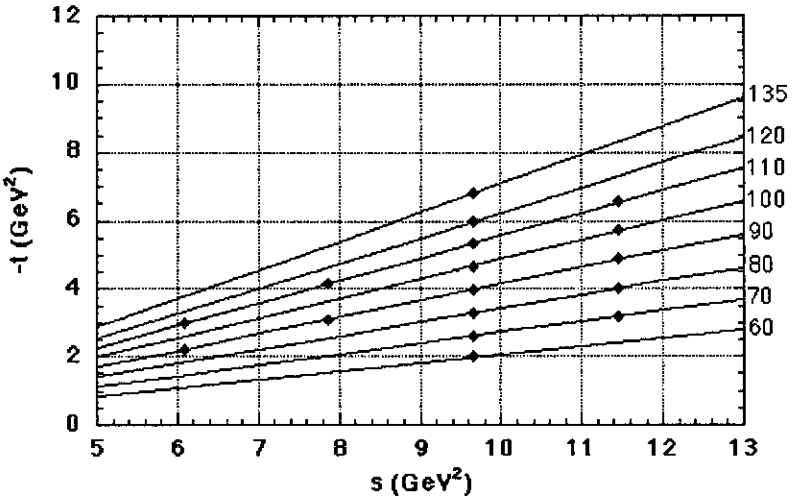

FIG. 7. Kinematics of Compton scattering. The lines indicate contours of constant θ_{cm}, whose value is indicated. The points are the proposed kinematics of the experiment.

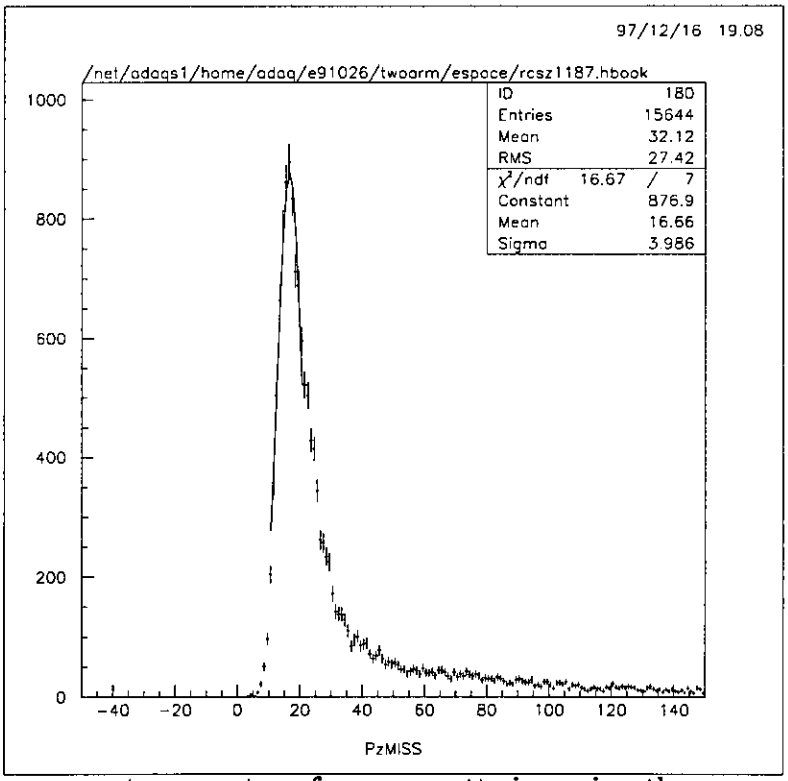

FIG. 8. Missing momentum spectum from *ep* scattering using the HRS pair in Hall A. The resolution from this plot implies angular resolutions $\sigma_\theta \approx \sigma_\phi \approx 0.9$ mr.

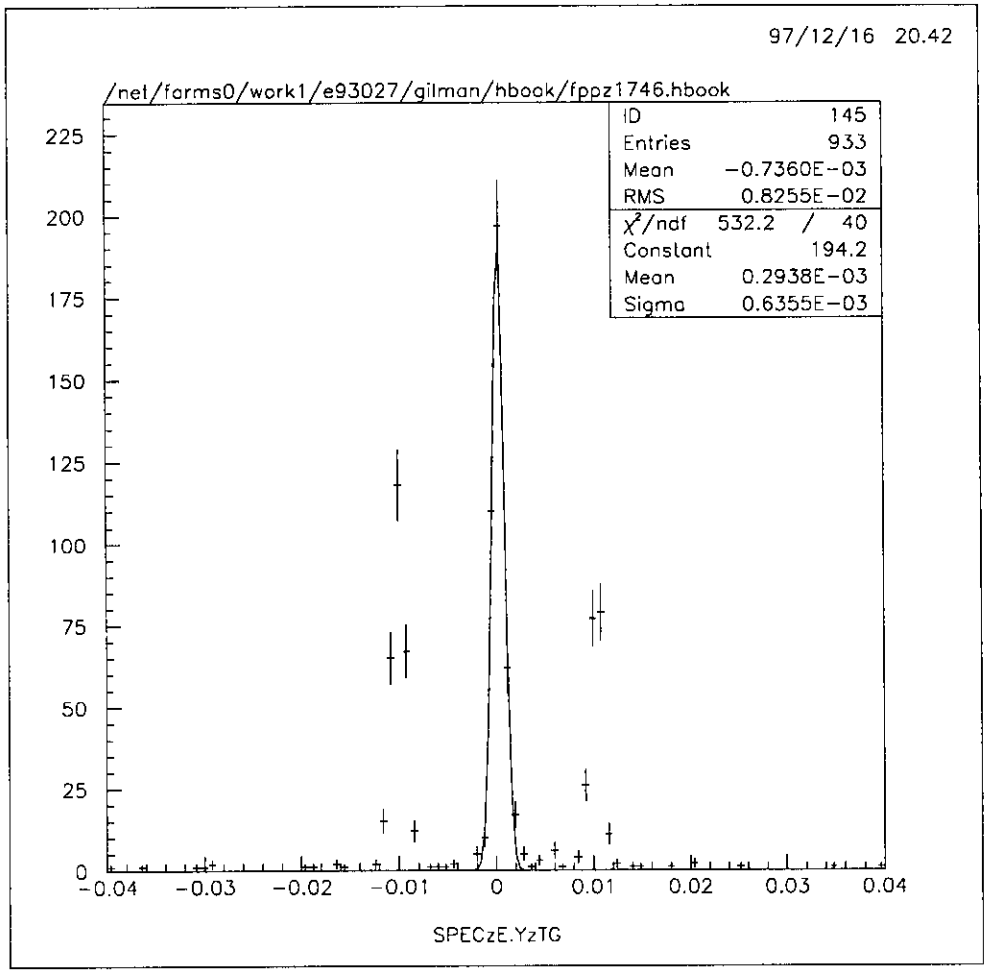

FIG. 9. A plot showing the y resolution (~ 0.7 mm) of the HRS.

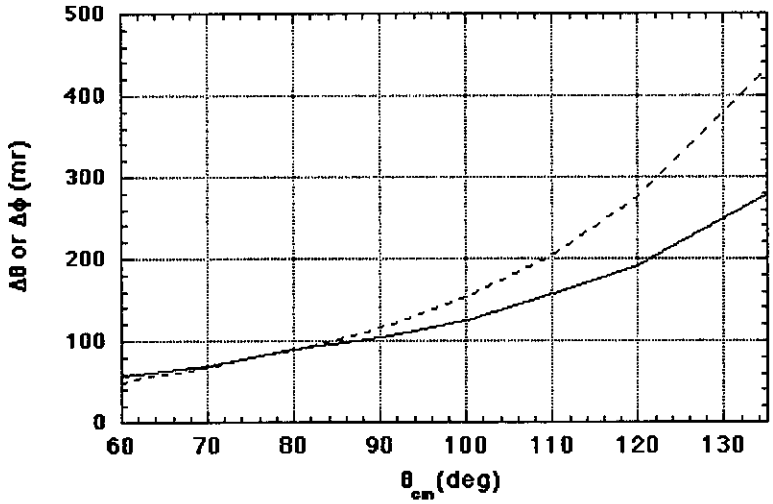

FIG. 10. The angular acceptance in the photon arm needed to match the acceptance in the proton arm as a function of center of mass scattering angle at 5 GeV

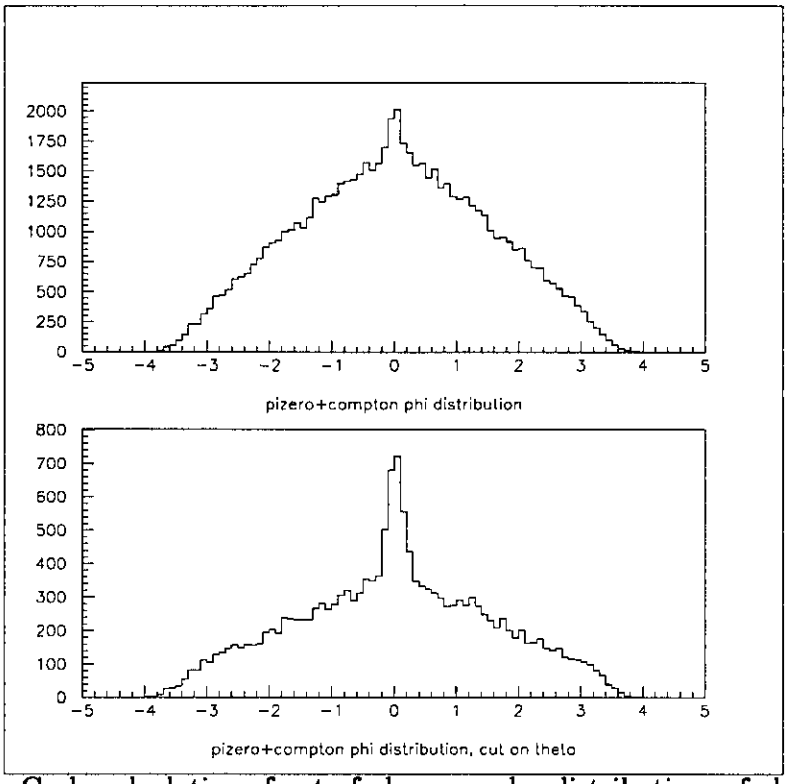

FIG. 11. Monte Carlo calculation of out-of-plane angular distributions of photons from Compton and π^0 photoproduction. The upper plot has no cuts while the lower plot has a 2-σ cut on the in-plane angle. The broad distribution is the π^0 cone, whereas the peak centered at 0 are the Compton photons. The calculations were done at E=6 GeV, θ_{cm}=110° using the angular resolutions shown in Table II.

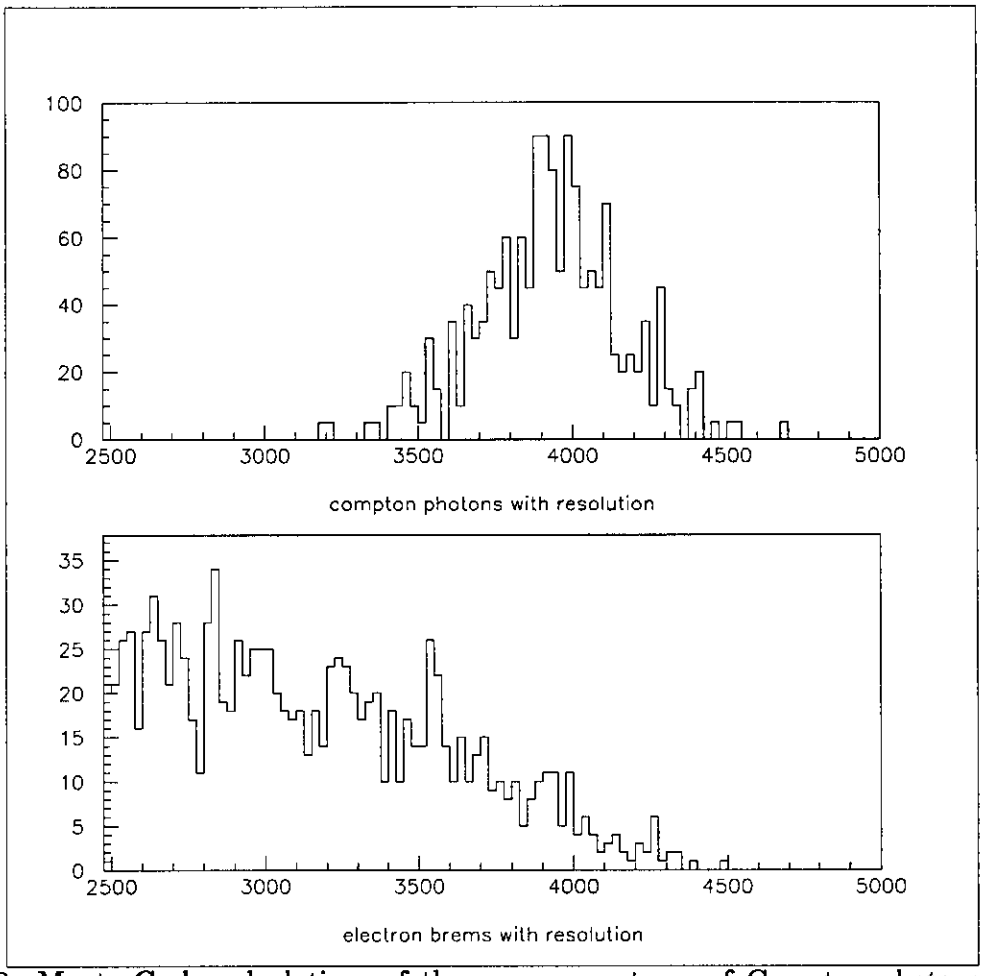

FIG. 12. Monte Carlo calculations of the energy spectrum of Compton photons (top) and $ep\gamma$ photons (bottom). The calculations were done at E=6 GeV, $\theta_{cm} = 70°$. The ratio of $ep\gamma$ to Compton events in the region above 3500 MeV is ~ 0.20.

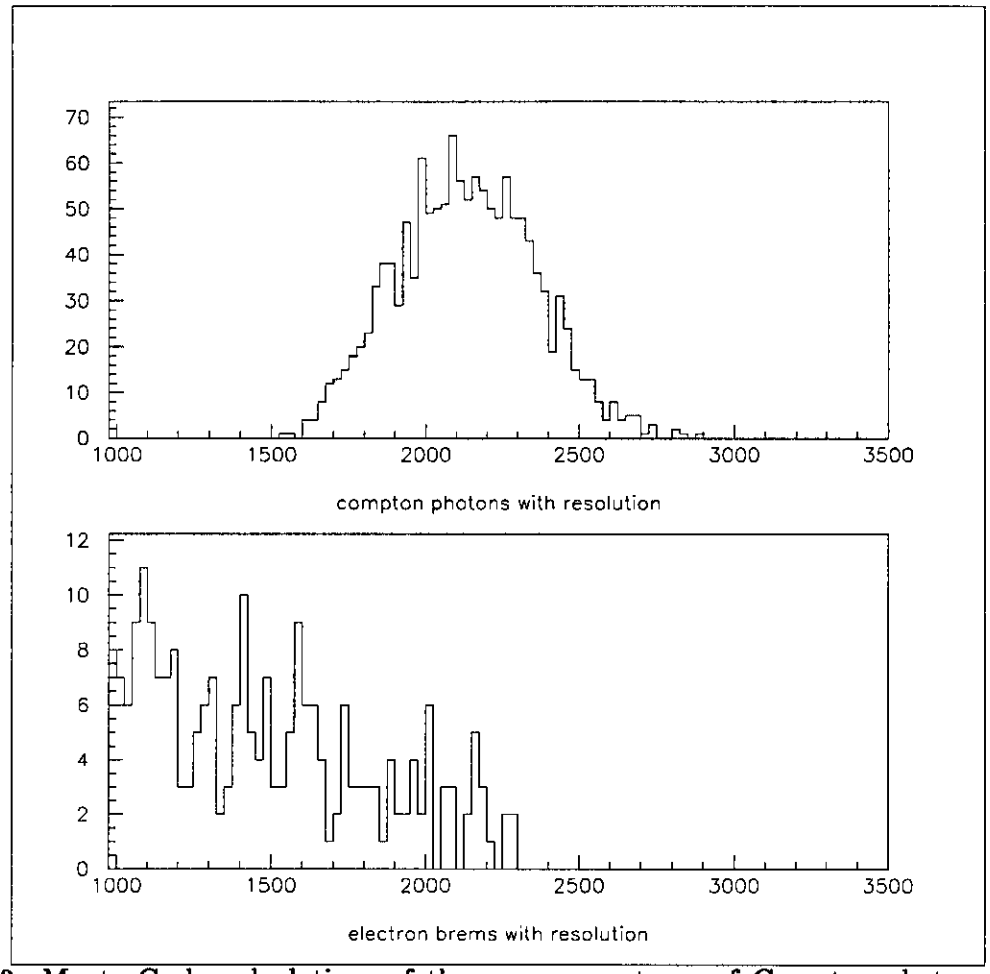

FIG. 13. Monte Carlo calculations of the energy spectrum of Compton photons (top) and $ep\gamma$ photons (bottom). The calculations were done at E=6 GeV, $\theta_{cm} = 110$ °. The ratio of $ep\gamma$ to Compton events in the region above 1500 MeV is ~ 0.06.

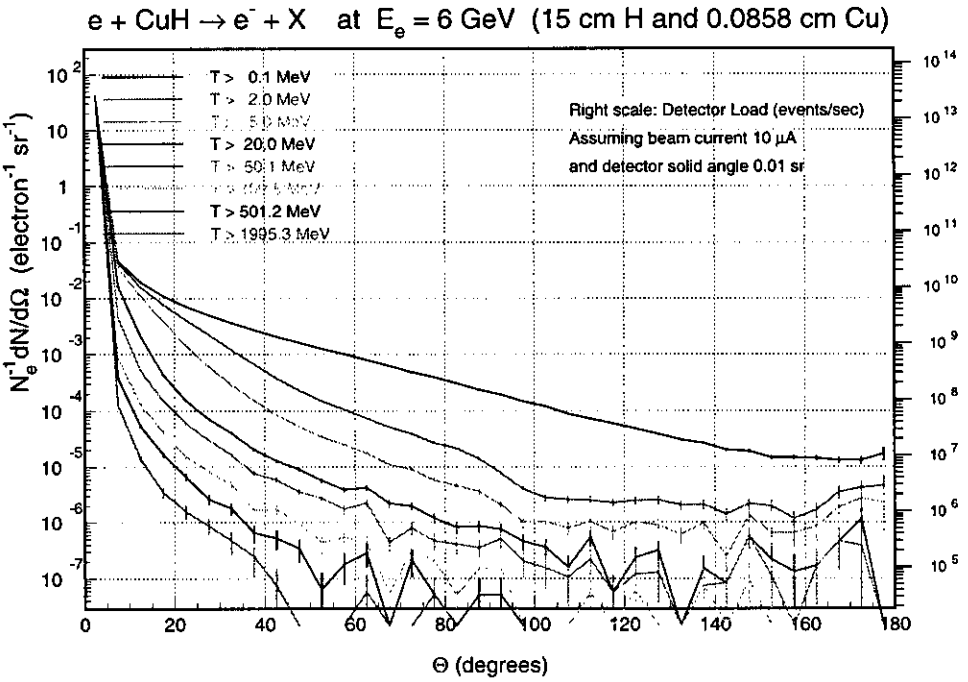

FIG. 14. Monte Carlo calculations of the electron background into a 10 msr solid angle as a function of energy threshold and angle when 10 μA of 6 GeV electrons is incident on a 6% copper radiator, followed by a 15-cm LH_2 target.

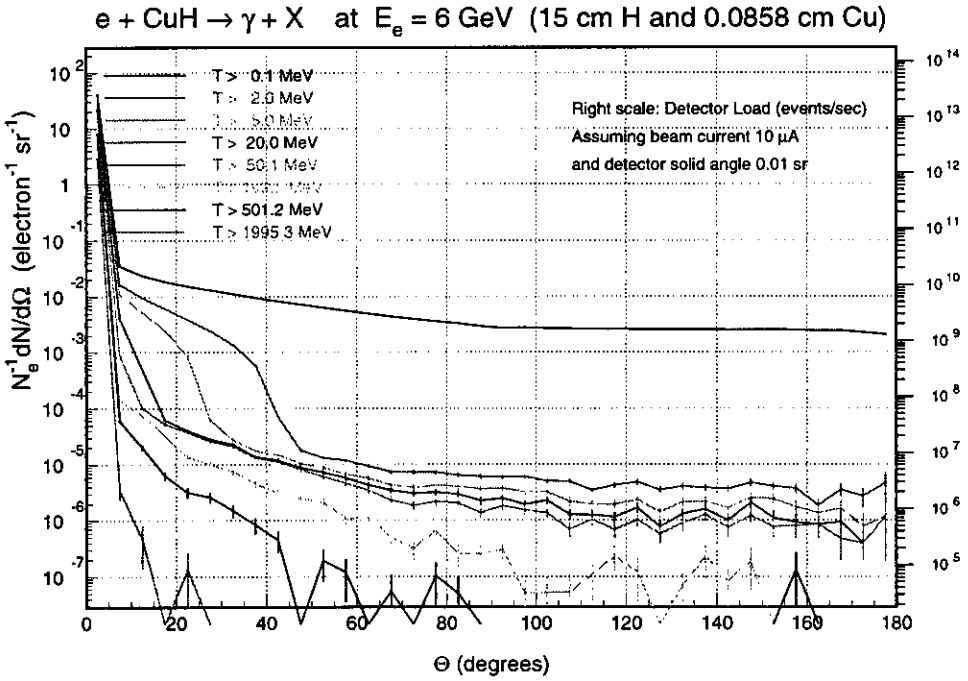

FIG. 15. Monte Carlo calculations of the photon background into a 10 msr solid angle as a function of energy threshold and angle when 10 μA of 6 GeV electrons is incident on a 6% copper radiator, followed by a 15-cm LH_2 target.